GeoScienceWorld
Lithosphere
Volume 2023, Article ID lithosphere_2023_186, 10 pages
https://doi.org/10.2113/2023/lithosphere_2023_186

Lithosphere

Research Article

Not Only Garnets…

Irina Galuskina,[1] **Evgeny Galuskin**,[1] **and Yevgeny Vapnik**[2]

[1]*Institute of Earth Sciences, Faculty of Natural Sciences, University of Silesia, Sosnowiec 41-200, Poland*
[2]*Department of Geological and Environmental Sciences, Ben-Gurion University of the Negev, P.O.B. 653, Beer-Sheva 84105, Israel*

Correspondence should be addressed to Irina Galuskina; irina.galuskina@us.edu.pl

Received 3 May 2023; Accepted 2 November 2023; Published 15 December 2023

Academic Editor: Marta Morana

Garnets have been known to man since time immemorial and are used in a wide variety of applications as well as being prototypes of useful synthetic materials. Our investigations show that in nature, garnets and minerals with a langasite-type structure can be very close in composition. Examples are cubic Ti-rich garnets with the common formula $Ca_3(Ti^{4+},Fe^{3+},Al)_2(Si,Fe^{3+},Al)_3O_{12}$ and the new trigonal mineral qeltite, $Ca_3Ti(Fe^{3+}{}_2Si)Si_2O_{14}$, which occur in paralavas of the pyrometamorphic Hatrurim Complex, Israel. Synthetic compounds of the langasite family are important because of their functional properties, such as unique piezoelectricity, high thermal stability, and low acoustic losses, as well as optical nonlinearity and multiferroicity. Qeltite is the first high-temperature terrestrial mineral with a langasite-type structure, the description of which was a catalyst for the discovery in pyrometamorphic rocks of the Hatrurim Complex of a whole series of new natural phases with langasite-type structure and varied composition ($A_3BC_3D_2O_{14}$, where A = Ca and Ba; B = Ti, Nb, Sb, and Zr; C = Ti, Al, Fe, and Si; and D = Si). We think that qeltite and other minerals with langasite-type structure may be relatively widely distributed in terrestrial rocks that form under similar conditions to those of Ti-rich garnet but are missed by researchers.

1. Introduction

Silicate garnets occur as rock-forming and accessory minerals in magmatic and metamorphic rocks and are often used as a source of petrogenetic information [1, 2]. Titanium-rich garnets occur in Si-undersaturated intrusive alkaline rocks, carbonatites, and pyrometamorphic and metasomatic rocks—calcic skarns and rodingites. Titanium-bearing garnet with the general formula $Ca_3(Ti^{4+},Fe^{3+},Al)_2(Si,Fe^{3+},Al)_3O_{12}$ and a TiO_2 content reaching 15–21 wt.% is often the main or an accessory mineral in melilite hornfelses and paralavas, which are widely distributed in the pyrometamorphic Hatrurim Complex in Israel [3, 4]. Another mineral similar in composition to Ti-rich garnets, with the composition $Ca_3Ti[(Fe^{3+},Al)_2(Ti^{4+},Si)]Si_2O_{14}$, but with a different type of structure (online supplementary Figure S1), was recently discovered in rocks of the Hatrurim Complex. This is the mineral qeltite, with the end-member formula $Ca_3Ti(Fe^{3+}{}_2Si)Si_2O_{14}$, which crystallizes in the noncentrosymmetric *P*321 space group [5]. Qeltite is the first terrestrial high-temperature mineral that is also an analog of an important group of synthetic compounds with the langasite-type structure. These phases are known for their physical properties, such as piezoelectricity, high thermal stability, and low acoustic losses, as well as optical nonlinearity and multiferroicity [6–11]. The name langasite is derived from the chemical composition of the synthetic compound $La_3Ga_5SiO_{14}$ [12]. Langasites are characterized by significant chemical diversity. At present, there are more than 200 phases with the langasite-type structure, and they are successfully used in different fields of science and technology [6, 9, 13–15]. Moreover, it is interesting to note that there are low-temperature minerals in the dugganite group, which are characterized by the noncentrosymmetric *P*321 space group [16]. These minerals inspired the synthesis of Te-bearing members of the langasite family featuring multiferroic properties [17]. The dugganite group combines four minerals: dugganite, $Pb_3Zn_3(AsO_4)_2(TeO_6)$, trigonal, P321 (#150), a = 8.460(2)

Å, c = 5.206(2) Å; cheremnykhite, $Pb_3Zn_3(VO_4)_2(TeO_6)$, orthorhombic, a = 8.58(3) Å, b = 14.86(5) Å, c = 5.18(3) Å; joëlbruggerite, $Pb_3Zn_3(Sb^{5+},Te^{6+})As_2O_{13}(OH,O)$, trigonal, P321 (#150), a = 8.4803(17) Å, c = 5.2334(12) Å; kuksite, $Pb_3Zn_3(PO_4)_2(TeO_6)$, trigonal, P321 (#150), a = 8.39 Å, c = 5.18 Å. They formed in oxidized pyrite-bearing metasomatite ores with gold-telluride mineralization [18] or in the oxidation zone of silver-lead and silver-polymetallic ores [19, 20].

Besides qeltite, there is one known natural extraterrestrial mineral with the langasite-type structure: paqueite, $Ca_3Ti(Al_2Ti)Si_2O_{14}$, which was discovered in a refractory inclusion within the Allende meteorite [21].

Due to the similar composition and physical properties (such as color and hardness) of Ti-rich garnets and Ti-Si-langasites from pyrometamorphic rocks of the Hatrurim Complex, the latter has received very little attention (online supplementary Figure S2). The discovery of "Ti-rich garnets" of an unusual flattened form in gehlenite paralava, and the subsequent discovery of qeltite, $Ca_3Ti(Fe^{3+}{}_2Si)Si_2O_{14}$ [5], as well as the detection of paqueite in phosphide-bearing breccia in the Hatrurim Basin [22], allowed for the study of garnet-like phases in the Hatrurim Complex from a different perspective. In this way, in this study, we were able to find more than ten potentially new minerals with the langasite-type structure, some of which exhibit unusual composition and contain Ba, Sb, Nb, and Zr.

In this paper, we present the results of an investigation into terrestrial minerals with the langasite-type structure which are intimately associated with the garnet of the Ti-rich andradite-schorlomite series. We provide data on mineral associations bearing langasites and discuss the question of their genesis. We interpret that langasite may be relatively widely distributed in terrestrial rocks as it forms under similar conditions to Ti-rich garnet but tends to be overlooked by researchers.

1.1. Methods of Investigation. The morphology and composition of minerals with the langasite-type structure and associated minerals were studied using a Phenom XL desktop scanning electron microscope (Institute of Earth Sciences, Faculty of Natural Sciences, University of Silesia, Sosnowiec, Poland) together with electron microprobe analysis (Cameca SX100, Institute of Geochemistry, Mineralogy and Petrology, University of Warsaw and the Polish Geological Institute—National Research Institute, Warszawa, Poland). Chemical analyses were carried out in the WDS-mode (wavelength-dispersive X-ray spectroscopy settings 15 keV, 20–40 nA, and 2 μm beam diameter) using the following lines and standards: Ca$K\alpha$—wollastonite and diopside; Mg$K\alpha$—diopside; Sr$L\alpha$—celestine; Ba$L\alpha$—baryte; Mn$K\alpha$—rhodonite; Cu$K\alpha$—cuprite and chalcopyrite; Zn$K\alpha$—sphalerite; Al$K\alpha$—orthoclase; Fe$K\alpha$—Fe_2O_3 and pentlandite; Cr$K\beta$—Cr_2O_3; Ti$K\alpha$—rutile; Zr$L\alpha$—zircon; Nb$L\alpha$—$LiNbO_3$; V$K\alpha$—V_2O_3, V_{met}; P$K\alpha$—YPO_4 and apatite; Sb$L\alpha$—InSb.

Raman spectra of the studied minerals with the langasite-type structure were recorded on a WITec alpha 300R Confocal Raman Microscope (Institute of Earth Sciences, Faculty of Natural Sciences, University of Silesia, Poland) equipped with an air-cooled solid laser (488 nm) and a CCD camera operating at −61°C. An air Zeiss LD EC Epiplan-Neofluar DIC-100/0.75 NA objective was used. Raman scattered light was focused on a broad band single-mode fiber with an effective pinhole size of approximately 30 μm and monochromator with a 1800 mm^{-1} grating. The power of the laser at the sample position was 20 mW. Integration times of 3 seconds with an accumulation of twenty scans were chosen and the resolution selected was 2 cm^{-1}. The monochromator was calibrated using the Raman scattering line of a silicon plate (520.7 cm^{-1}).

2. Results and Discussion

2.1. Hatrurim Complex. Pyrometamorphic rocks of the Hatrurim Complex, in which minerals of the langasite-type structure were found, are unique deposits whose genesis involved high temperatures and low pressures (sanidinite facies). As a result, various mineral associations—among them oxidized associations bearing diverse ferrites—are predominant, and there are also very rare reduced mineral associations featuring minerals such as osbornite and phosphides, which are typical of meteorites [22–24]. The mineral diversity of the Hatrurim Complex rocks is connected with the high chemical inhomogeneity of the sedimentary protolith, multistage formation, and the complexity of the rock thermal alteration processes as a result of natural fires. Rocks of the Hatrurim Complex, including spurrite, gehlenite, and larnite-bearing rocks, together with paralavas of variable composition, make up a large area in the zone along the Dead Sea Rift in the territories of Palestine, Israel, and Jordan (online supplementary Figure S3)[25].

However, the genesis of the Hatrurim Complex so far remains an enigma. There are two hypotheses, but neither is able to explain all the particularities of these complex rocks. The first "classic" hypothesis proposes that sedimentary rocks underwent high-temperature alteration as a result of organic fuel (bitumen) combustion within the protolith [26, 27]. The other, younger, "mud volcano" hypothesis assumes that high-temperature alteration of the sedimentary protolith took place under the influence of methane, which was delivered to the area from the tectonically active zone of the Dead Sea Rift [28].

2.2. Natural Langasites in Rocks of the Hatrurim Complex. Minerals with the langasite-type structure were found in paralava from Nabi Musa, Palestine, and a few localities in the Hatrurim Basin, Israel (online supplementary Figure S3). About ten isostructural phases were found, among which paqueite, $Ca_3TiSi_2(Al_2Ti)O_{14}$, which was described by Ma et al. [21] and recently approved by the CNMNC-IMA, and qeltite, $Ca_3TiSi_2(Fe_2Si)O_{14}$ [5], are known mineral species (Table 1). Iron-free paqueite was identified in phosphide-bearing breccia at the contact of the reduced gehlenite-bearing paralava and altered fragments of the country rocks (transformed by later processes to

Table 1 New and potentially new minerals of langasite-type structure with the general formula $A_3BC_3D_2O_{14}$ from the Hatrurim Complex.

Site	A_3	B	C_3	D_2	O_{14}	Mineral	End member %	Synthetic analog
1	Ca_3	Ti^{4+}	$Ti^{4+}Al_2$	Si_2	O_{14}	Paqueite	~60%	Yes
2	Ca_3	Ti^{4+}	$SiFe^{3+}{}_2$	Si_2	O_{14}	Qeltite	~70%	No
3	Ca_3	Ti^{4+}	$Ti^{4+}Fe^{3+}{}_2$	Si_2	O_{14}	Potentially new	~60%	No
4	Ca_3	Ti^{4+}	$SiAl_2$	Si_2	O_{14}	Potentially new	~55%	Yes
5	Ba_3	Nb^{5+}	$Fe^{3+}{}_3$	Si_2	O_{14}	Potentially new	~80%	Yes
6	Ba_3	Ti^{4+}	$SiFe^{3+}{}_2$	Si_2	O_{14}		~35%	No
7	Ba_3	Ti^{4+}	$SiAl_2$	Si_2	O_{14}		~14%	No
8	Ba_3	Sb^{5+}	$Fe^{3+}{}_3$	Si_2	O_{14}		~30%	Yes
9	Ba_3	Sb^{5+}	Al_3	Si_2	O_{14}		~14%	No
10	Ba_3	Zr	$SiFe^{3+}{}_2$	Si_2	O_{14}		~30%	No
11	Ba_3	Zr	$SiAl_2$	Si_2	O_{14}		~14%	No
12	Ca_3	Sb^{5+}	Al_3	Si_2	O_{14}	Potentially new	~60%	No
13	Ca_3	Sb^{5+}	$Fe^{3+}{}_3$	Si_2	O_{14}		~17%	Yes
14	Ca_3	Nb^{5+}	$Fe^{3+}{}_3$	Si_2	O_{14}		~10%	No
13	Ca_3	Nb^{5+}	Al_3	Si_2	O_{14}		~10%	Yes

hydrogrossular-bearing rock) in the Negev Desert (Figure 1(a) and 1(b); Figure 2(a); online supplementary Figure S3) [22]. Iron-bearing paqueite and other langasites were found in small veins of coarse-grained paralavas within melilite massive hornfelses. These paralavas are composed of melilite of the gehlenite-akermanite-alumoakermanite series, together with rankinite, wollastonite, and garnet of the andradite-schorlomite series, fluorapatite, and larnite-flamite (Figure 2(b)). Pyroxenes of the diopside-esseneite series and minerals of the latiumite-levantite series appear more rarely (Figure 2(c)). In these paralavas, flattened langasite crystals are confined to oval polymineral inclusions 0.1–0.3 mm in size in the rock-forming minerals, mainly in rankinite and wollastonite (Figure 1).

In a Si-Ti-R^{3+} (Fe^{3+} + Al) ternary diagram, most schorlomite-like langasites (Table 2) form a compact field, and Ti-rich garnet also falls within this field (Figure 3). This garnet is characterized by the mean empirical formula $(Ca_{2.93}Mg_{0.05}Na_{0.02})_{\Sigma 3}(Ti_{1.04}Fe^{3+}{}_{0.79}Mn^{2+}{}_{0.09}Fe^{2+}{}_{0.05}Mg_{0.02}Nb^{5+}{}_{0.01})_{\Sigma 2}(Si_{2.03}Al_{0.51}Fe^{3+}{}_{0.41}V^{5+}{}_{0.03}P^{5+}{}_{0.02})_{\Sigma 3}O_{12}$, where the main end members of andradite, hatcheonite, and schorlomite amount to about 40%, 25%, and 20% wt. %, respectively (Table 3). Formally, this garnet should be classified as ferric hatcheonite, which is known only from meteorites [29] because the sum of the titanium end members is higher than the amount of andradite. The general formula of Ti-langasite can be presented as $^{A}Ca_3{}^{B}Ti^{4+}{}^{C}(R^{3+}{}_2\,R^{4+})^{D}Si_2O_{14}$. When the C site is occupied by (Al_2Ti), it is classified as paqueite, and when it is occupied by (Fe_2Si), it is classified as qeltite, and when it is occupied by (Al_2Si) or (Fe_2Ti), it is a potentially new mineral (Table 1).

The discovery of langasite containing Ba, Sb, Nb, and Zr was unexpected. These elements are confined to polymineral inclusions in wollastonite or rankinite, where they form crystals with hexagonal or orthogonal cross-sections (Figure 4). Three potentially new minerals containing exotic elements were found (Table 4). The first has the empirical formula $Ba_{2.99}(Ti_{0.36}Sb^{5+}{}_{0.32}Zr_{0.29}U^{6+}{}_{0.02}Nb^{5+}{}_{0.01})_{\Sigma 1.00}(Fe^{3+}{}_{2.06}Al_{0.41}Si_{0.36}Ti^{4+}{}_{0.18}V^{5+}{}_{0.01})_{\Sigma 3.02}Si_2O_{14}$, which can be formally simplified based on the dominant valence rule to the end-member formula $Ba_3Ti^{4+}SiFe^{3+}{}_2Si_2O_{14}$. A determination of the possible end members in this formula gives five more end members with contents higher than 10%: $Ba_3Ti^{4+}SiAl_2Si_2O_{14}$, $Ba_3ZrSiFe^{3+}{}_2Si_2O_{14}$, $Ba_3ZrSiAl_2Si_2O_{14}$, $Ba_3Sb^{5+}Fe^{3+}{}_3Si_2O_{14}$, and $Ba_3Sb^{5+}Al_3Si_2O_{14}$. This indicates that these new minerals are close in composition to the end members that can be found in nature. The second exotic langasite has the empirical formula $(Ba_{2.83}Ca_{0.14}Na_{0.03}Sr_{0.02})_{\Sigma 3.02}(Nb^{5+}{}_{0.86}Ti^{4+}{}_{0.05}Fe^{2+}{}_{0.04}Mn_{0.05})_{\Sigma 1.00}(Fe^{3+}{}_{2.44}Ti^{4+}{}_{0.23}Al_{0.18}Si_{0.14})Si_2O_{14}$, and formally, it can be described by the end-member formula $Ba_3Nb^{5+}Fe^{3+}{}_3Si_2O_{14}$ (~80%). The third exotic langasite has the empirical formula $(Ca_{2.89}Y_{0.04}Sr_{0.04}Mn^{2+}{}_{0.02})_{\Sigma 2.99}(Sb^{5+}{}_{0.62}Nb^{5+}{}_{0.17}Ti^{4+}{}_{0.14}Fe_{0.07})_{\Sigma 1.00}(Al_{2.32}Fe^{3+}{}_{0.51}Si_{0.20})_{\Sigma 3.03}Si_2O_{14}$ and has the ideal end-member formula $Ca_3Sb^{5+}Al_3Si_2O_{14}$. The last phase contains three additional end members that make up more than 10% of its composition: $Ca_3Sb^{5+}Fe^{3+}{}_3Si_2O_{14}$, $Ca_3Nb^{5+}Fe^{3+}{}_3Si_2O_{14}$, and $Ca_3Nb^{5+}Al_3Si_2O_{14}$. Thirteen new and potentially new langasite-type minerals are listed in Table 1.

Exotic langasites are, as a rule, confined to aggregates bearing rare and new minerals. For instance, Ba-Nb-langasite associates with fresnoite, hexacelsian, mazorite, barioferrite, gurimite, and a potentially new mineral—a Ba-analog of powellite (Figure 4(a)).

Structural data were obtained for qeltite ($a = b$ = 8.0077[5] Å, c = 4.9956[4] Å; α = β = 90°, γ = 120°, V = 277.42[4] Å^3, and Z = 1) from pyroxene-bearing

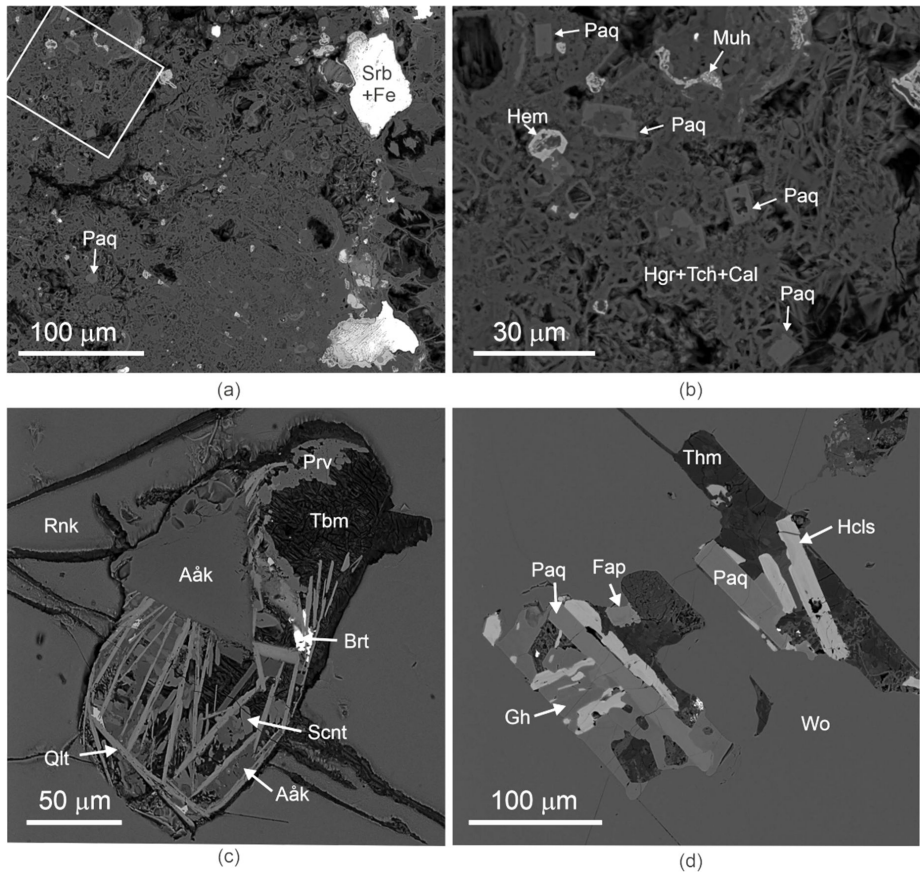

FIGURE 1: Langasites of $CaO\text{-}Al_2O_3\text{-}Fe_2O_3\text{-}TiO_2\text{-}SiO_2$ system. (a) Strongly altered contact of a country-rock clast and gehlenite-bearing paralava marked by schreibersite and native iron aggregates. The fragment magnified in Figure 2 (b) is outlined by an inset frame. (b) Relics of paqueite crystals in a porous rock. (c) Aggregates of flattened crystals of a Al analog of qeltite. (d) Crystals of ferric paqueite in aggregates containing hexacelsian. Aåk—alumoåkermanite, Brt—barite, Cal—calcite, Fap—fluorapatite, Gh—gehlenite, Hcls—hexacelsian, Hem—hematite, Hgr—hydrogrossular, Muh—murashkoite, Qlt—qeltite, Paq—paqueite, Rnk—rankinite, Scb—schreibersite, Scnt—silicocarnotite, Tbm—tobermorite, Tch—tacharanite, and Wo—wollastonite.

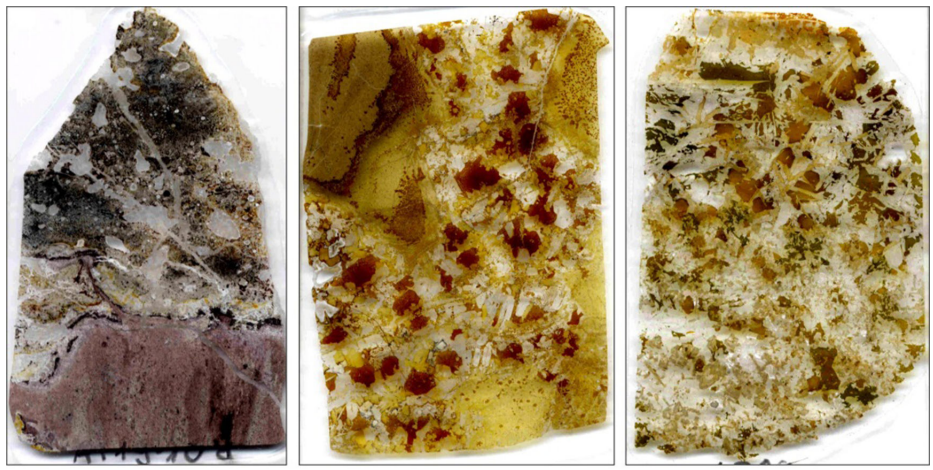

FIGURE 2: Petrographic thin sections of the main types of paralava in which langasites were found. (a) Phosphide-bearing breccia, contact of dark amygdaloidal gehlenite-flamite-bearing paralava with an altered country-rock clast. (b) Gehlenite-andradite-bearing coarse-grained paralava with fragments of fine-grained gehlenite-bearing hornfels. (c) Gehlenite-esseneite-bearing paralava with the minerals of the latiumite-levantite series. Gehlenite—yellow; garnet of the andradite-schorlomite series—dark brown; wollastonite, rankinite, cuspidine, fluorapatite, and latiumite-levantite—white and colorless; and esseneite—dirty green.

Table 2: Chemical composition of langasite of the CaO-Al_2O_3-Fe_2O_3-TiO_2-SiO_2 system: 1—Fe-free paqueite, phosphide-bearing breccia, wadi Zohar, Negev; 2—Fe-bearing paqueite, esseneite-bearing paralava, wadi Halamish tributary, Negev; 3—Fe-analog of paqueite, ranknite-bearing paralava, wadi Halamish, Negev; 4—qeltite, wollastonite-bearing paralava, Nabi Musa, Palestine; and 5—Al-analog of qeltite, esseneite-bearing paralava, Har Ye'elim, Negev.

	1			2			3			4			5
	$n = 7$	SD	Range	$n = 11$	SD	Range	$n = 16$	SD	Range	$n = 9$	SD	Range	$n = 3$
MgO	0.10	0.04	0.07–0.17	0.05	0.01	0–0.07	n.d.			n.d.			n.d.
CaO	30.25	0.12	30.05–30.40	29.23	0.28	28.96–29.44	27.34	0.26	26.83–27.76	28.79	0.18	28.38–29.04	29.44
SrO	0.21	0.01	0.19–0.24	0.12	0.05	0–0.23	0.48	0.09	0.37–0.66	0.27	0.12	0.12–0.42	0.16
BaO	n.d.			0.47	0.41	0.25–0.81	0.20	0.10	0.07–0.42	0.00	0.11	0–0.27	0.29
FeO							2.27	0.49	1.06–2.96				0.32
Fe_2O_3	0.16	0.02	0–0.23	10.63	8.97	9.47–12.46	15.47	0.71	14.65–17.13	18.71	0.41	18.14–19.30	5.77
Al_2O_3	18.88	0.52	18.35–19.79	11.56	3.68	10.67–12.40	5.57	0.32	5.14–6.06	5.39	0.23	5.12–5.67	14.33
Cr_2O_3	0.08	0.03	0.04–0.13	n.d.			0.07	0.03	0–0.12	0.20	0.05	0.10–0.30	0.00
SiO_2	25.25	1.03	24.40–26.96	25.49	2.97	24.56–26.44	23.59	0.60	22.51–24.82	26.60	0.50	25.73–27.24	26.83
TiO_2	23.26	1.78	20.65–25.05	21.63	6.41	19.99–22.59	23.40	0.65	22.09–24.33	18.47	0.61	17.51–19.55	20.41
ZrO_2	n.d.			n.d.			0.14	0.06	0.06–0.32	0.20	0.08	0.11–0.35	0.00
Nb_2O_5	n.d.			0.15	0.01	0.10–0.20	0.06	0.04	0.02–0.17	0.00			0.40
V_2O_5	n.d.			n.d.			n.d.			0.00			0.13
P_2O_5	n.d.			n.d.			0.22	0.14	0.08–0.60	0.00			0.00
Total	98.19			99.33			98.81			98.63			98.08
Ca	2.99			2.97			2.89			3.02			2.97
Na													
Mg	0.01			0.01									
Sr	0.01			0.01			0.03			0.02			0.01
Ba				0.02			0.01						0.01
Fe^{2+}							0.07						0.03
A	***3.01***			***3.01***			***3.00***			***3.04***			***3.02***
Ti^{4+}	0.99			0.99			0.86			0.97			0.98
Zr							0.01			0.01			
Nb^{5+}				0.01									0.02
Fe^{2+}							0.12						
Cr^{3+}	0.01						0.01			0.02			
B	***1***			***1***			***1***			***1***			***1***
Fe^{3+}	0.01			0.76			1.15			1.38			0.41
Al	2.05			1.29			0.65			0.62			1.59
Si	0.33			0.41			0.35			0.60			0.53
Ti^{4+}	0.62			0.55			0.88			0.39			0.44
C	***3.01***			***3.01***			***3.03***			***2.99***			***2.97***
Si	2			2			1.98			2			1.99
P^{5+}							0.02						
V^{5+}													0.01
D	***2***			***2***			***2***			***2***			***2***

paralava at Nabi Musa, Palestine. Its structure corresponds to the langasite archetype characterized by the noncentrosymmetric space group and effects of structural disordering lead to the appearance of right and left forms—paqueite and qeltite, respectively [5, 21, 30] (online supplementary Figure S4).

Langasites have characteristic Raman spectra in which, as distinct from garnets of similar composition, the

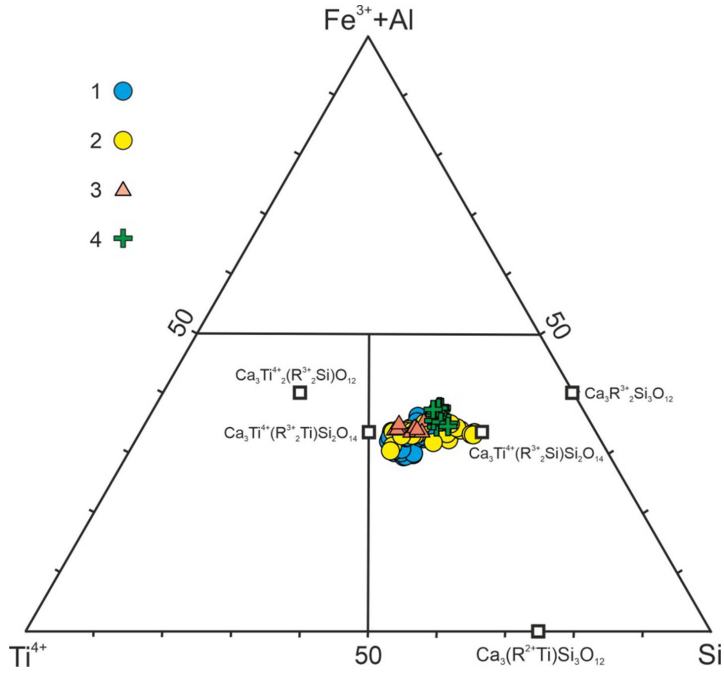

Figure 3: Si–(Fe^{3+}+Al)–Ti^{4+} ternary plot displaying langasite and Ti-rich garnet compositions: 1—langasites from paralava, Negev Desert; 2—langasites from paralava, Palestine; 3—paqueite from phosphide-bearing breccia, Negev Desert; and 4—Ti-rich garnet from paralava, Negev Desert.

Table 3: Chemical analyses of Ti-rich garnet in association with the Al-analog of qeltite.

	$n = 7$	SD	Range		Atom per formula unit
Na_2O	0.12	0.04	0.07–0.17	Ca	2.93
MgO	0.56	0.18	0.32–0.83	Na	0.02
CaO	31.73	0.20	31.50–31.99	Mg	0.05
FeO	0.66	0.36	0–0.98	***X***	***3.00***
MnO	1.26	0.12	1.16–1.50	Ti^{4+}	1.04
Fe_2O_3	18.42	0.72	17.86–19.62	Fe^{3+}	0.79
Al_2O_3	5.01	0.27	4.57–5.33	Mn^{2+}	0.09
SiO_2	23.50	0.08	23.42–23.61	Fe^{2+}	0.05
TiO_2	16.04	0.44	15.46–16.60	Mg	0.02
Nb_2O_5	0.14	0.03	0.10–0.18	Nb^{5+}	0.01
V_2O_5	0.51	0.05	0.42–0.56	***Y***	***2.00***
P_2O_5	0.34	0.13	0.11–0.49	Si	2.03
Total	98.28			Fe^{3+}	0.41
				Al	0.51
				P^{5+}	0.02
				V^{5+}	0.03
				Z	***3.00***

$(Ca_{2.93}Mg_{0.05}Na_{0.02})_{\Sigma 3.00}(Ti_{1.04}Fe^{3+}_{0.79}Mn^{2+}_{0.09}Fe^{2+}_{0.05}Mg_{0.02}Nb^{5+}_{0.01})_{\Sigma 2.00}(Si_{2.03}Al_{0.51}Fe^{3+}_{0.41}\ V^{5+}_{0.03}P^{5+}_{0.02})_{\Sigma 3.00}O_{12}$.

strong bands are related to metal-oxygen vibrations at an octahedral site at about 600 cm^{-1} (Figure 5). The exotic langasites could be clearly identified with the help of Raman spectroscopy, and their spectra are analogous to the spectra of synthetic analogs (Figure 5) [31].

2.3. Genesis of Natural Langasites. The authors of the recently discovered refractory mineral paquetite in Ca-Al-rich inclusions from carbonaceous chondrite Allende CV3 hypothesized that it originated through condensation as a result of the reaction of gehlenite with vapor [21]. Con-

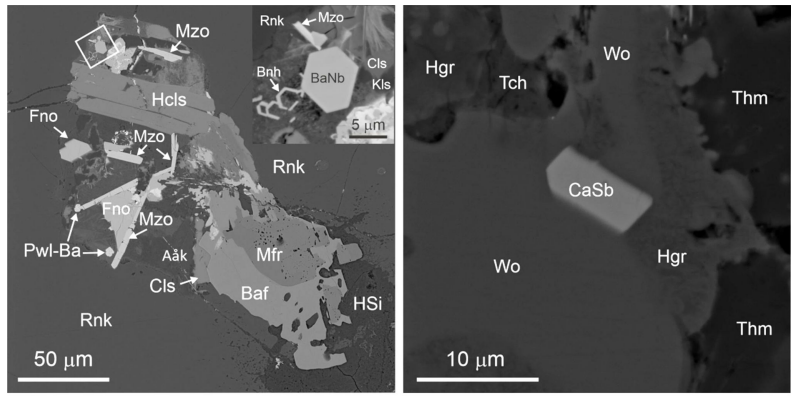

FIGURE 4: (a) Hexagonal crystal of Ba-Nb-langasite (frame magnified in inset) in association with rare Ti- and Ba-bearing minerals. (b) Orthogonal crystal (cross-section ~ parallel to *Z*) of Ca-Sb-langasite in an aggregate of secondary minerals with hexacelsian relics. Aåk—alumoåkermanite, Baf—barioferrite, BaNb—Ba-Nb-langasite, Bnh—benesherite, CaSb—Ca-Sb-langasite, Cls—celsian, Fno—fresnoite, Hcls—heksacelsian, Hgr—hydrogrossular, HSi—hydrated Ca-silicate, Kls—kalsilite, Mfr—magnesioferrite, Mzo—mazorite, Pwl-Ba—Ba-analog of powellite, Rnk—rankinite, Tch—tacharanite, Thm—thomsonite, and Wo—wollastonite.

TABLE 4: Chemical composition of exotic langasites: 1—Ba-Ti-dominant, 2—Ba-Nb-dominant, and 3—Ca-Sb-dominant.

	1	2			3		1	2	3
	$n = 3$	$n = 5$	SD	Range	$n = 2$		Atom per formula unit		
Na_2O	n.d.	0.09	0.01	0.07–0.10	n.d.	Ba	2.99	2.83	
CaO	n.d.	0.88	0.17	1.24–1.71	26.62	Ca		0.14	2.89
MnO	n.d.	0.42	0.34	0.17–1.00	0.25	Mn^{2+}			0.02
SrO	n.d.	0.22	0.03	0.17–0.26	0.63	Sr		0.02	0.04
BaO	49.26	47.58	0.54	46.89–48.15	n.d.	Na		0.03	
FeO	n.d.	0.31	n.d.		n.d.	Y			0.04
Al_2O_3	2.25	0.98	0.07	0.86–1.03	19.47	***A***	***2.99***	***3.02***	***2.99***
Fe_2O_3	17.66	21.36	0.29	21.05–21.73	7.63	Ti^{4+}	0.36	0.05	0.14
Y_2O_3	n.d.	n.d.			0.74	Zr	0.29		
SiO_2	15.23	14.14	0.26	13.93–14.58	21.69	Nb^{5+}	0.01	0.86	0.17
TiO_2	4.67	2.42	0.19	2.23–2.65	1.82	Sb^{5+}	0.32		0.62
ZrO_2	3.85	n.d.			n.d.	U^{6+}	0.02		
V_2O_5	0.13	n.d.			n.d.	Mn^{2+}		0.05	
Nb_2O_5	0.15	12.50	0.00	12.50–12.50	3.63	Fe^{2+}		0.04	
Sb_2O_5	5.53	n.d.			16.48	Fe^{3+}			0.07
UO_3	0.51	n.d.			n.d.	***B***	***1.00***	***1.00***	***1.00***
Total	99.23	100.89			98.96	Ti^{4+}	0.18	0.23	
						Al	0.41	0.18	2.32
						Fe^{3+}	2.06	2.44	0.51
						Si	0.36	0.14	0.20
						V^{5+}	0.01		
						C	***3.02***	***2.99***	***3.03***
						D/Si	2.00	2.00	2.00

[1]$Ba_{2.99}(Ti_{0.36}Sb^{5+}_{0.32}Zr_{0.29}U^{6+}_{0.02}Nb^{5+}_{0.01})_{\Sigma 1.00}(Fe^{3+}_{2.06}Al_{0.41}Si_{0.36}Ti^{4+}_{0.18}\ V^{5+}_{0.01})_{\Sigma 3.02}Si_2O_{14}$.

[2]$(Ba_{2.83}Ca_{0.14}Na_{0.03}Sr_{0.02})_{\Sigma 3.02}(Nb^{5+}_{0.86}Ti^{4+}_{0.05}Fe^{2+}_{0.04}Mn_{0.05})_{\Sigma 1.00}(Fe^{3+}_{2.44}Ti^{4+}_{0.23}Al_{0.18}Si_{0.14})Si_2O_{14}$.

[3]$(Ca_{2.89}Y_{0.04}Sr_{0.04}Mn^{2+}_{0.02})_{\Sigma 2.99}(Sb^{5+}_{0.62}Nb^{5+}_{0.17}Ti^{4+}_{0.14}Fe_{0.07})_{\Sigma 1.00}(Al_{2.32}Fe^{3+}_{0.51}Si_{0.20})_{\Sigma 3.03}Si_2O_{14}$.

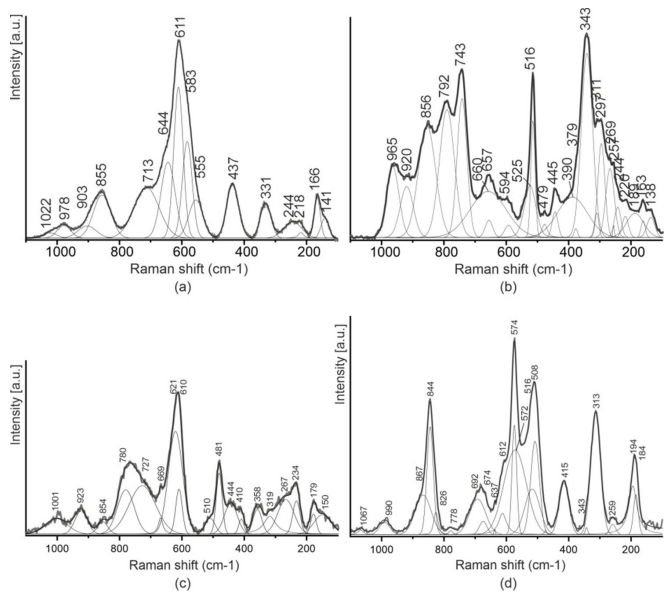

Figure 5: Raman spectra of qeltite (a) and Ti-rich garnet with a similar composition (b). (c) Paqueite Raman spectrum. (d) Ba-Nb-langasite Raman spectrum.

densation is the leading process in the formation of solid components from hot solar gas. The composition of the solid substances is controlled by the condensation temperature of the gaseous components. Early condensates include the so-called calcium- and aluminum-rich inclusions in which paqueite was found [32].

The genesis of terrestrial langasites from the Hatrurim Complex is connected with paralavas generated at high temperatures (>1200°C) and low pressures. Iron-free paqueite formed at the hot contact of melilite paralava under super-reduced conditions, as is confirmed by its association with osbornite [22, 23] (Figure 1(a) and 1(b)). All other studied langasites contain Fe^{3+} and are observed in polymineral aggregates, which are embedded in rock-forming minerals of paralava in the form of small, rounded inclusions (Figure 1(c) and 1(d)). These inclusions are products of the crystallization of residual melt microportions enriched in P, Ti, Ba, U, Zr, Sb, Nb, and V, which—in limited amounts—can be incorporated into rock-forming minerals such as wollastonite, gehlenite, rankinite, garnet, and flamite-larnite.

Both meteoritic and terrestrial langasites form at high temperatures. Synthetic langasite-family single crystals are mainly grown from a melt by the Czochralski method at 1470°C ± 20°C [10]. It follows that we can expect to find more natural langasites in magmatic and metamorphic rocks.

Data Availability

All data generated during this study are included in this published article and its supplementary materials. Original data are available on request from the corresponding author.

Conflicts of Interest

The authors declare that there is no conflict of interest regarding the publication of this paper.

Acknowledgments

These investigations were supported by a National Science Center of Poland Grant [grant number 2021/41/B/ST10/00130].

Supplementary Materials

Figure S1. (a) Schorlomite structure, $Ca_3Ti_2(Fe^{3+}2Si)O_{12}$ (one layer is shown), formed by Ca-polyhedra columns (hatched dark-yellow) and Ti^{4+}-octahedra (hatched green), between which there are (Fe^{3+},Si)-tetrahedra (blue). Regular, *Ia-3d*, a ≈ 12.15 Å [2]. (b) Qeltite structure, $Ca_3Ti(Fe^{3+}{}_2Si)Si_2O_{14}$, composed of two types of layers: a tetrahedral layer built from (Fe^{3+},Si)-tetrahedra (sea-green) and Si-tetrahedra (blue), and a layer formed by Ca-polyhedra (hatched dark-yellow) and Ti^{4+}-octahedra (hatched green). Projections on (001). Trigonal, *P*321, a = 8.008 Å, b = 8.008 Å, c = 4.996 Å [5]. Figure S2. BSE images and EDS spectra of schorlomite (a), qeltite (b) and paqueite (a). White circles indicate points of EDS analyses. Figure S3. (a) Outcrops of the Hatrurim Complex in Israel, Palestine and Jordan, shown by black spots with the exception of localities where natural langasites were found: the Hatrurim Basin and Nabi Musa – red spots. (b) The Hatrurim Basin; red circles are localities with langasite finds. 31 and 258 are numbers of roads (modified [25]). Figure S4. Fragments of natural langasite structures exhibiting enantiomorphism: (a) right paqueite, (b) left qeltite.

References

[1] A. R. Chakhmouradian and C. A. McCammon, "Schorlomite: a discussion of the crystal chemistry, formula, and inter-species boundaries," *Physics and Chemistry of Minerals*, vol. 32, no. 4, pp. 277–289, 2005.

[2] E. Schingaro, M. Lacalamita, E. Mesto, et al., "Crystal chemistry and light elements analysis of TI-rich Garnets," *American Mineralogist*, vol. 101, no. 2, pp. 371–384, 2016.

[3] I. O. Galuskina, E. V. Galuskin, A. S. Pakhomova, et al., "Khesinite, $Ca^{4}Mg^{2}Fe^{3+}{}_{10}O_4[(Fe^{3+}{}_{10}SI_2)O_{36}]$, a new rhönite-group (Sapphirine Supergroup) mineral from the Negev desert, Israel – natural analogue of the SFCA phase," *European Journal of Mineralogy*, vol. 29, no. 1, pp. 101–116, 2017.

[4] A. Krzątała, B. Krüger, I. Galuskina, Ye. Vapnik, and E. Galuskin, "Walstromite, $Baca_2(Si_3O_9)$, from rankinite paralava within Gehlenite Hornfels of the Hatrurim Basin, Nagev desert, Israel," *Minerals*, vol. 10, no. 5, p. 407, 2020.

[5] M. Galuskina, Y. Stachowicz, G. Vapnik, K. Zieliński, and K. Woźniak, "A potentially new mineral, $Ca_3Tisi_2(Fe^{3+}{}_2Si)O_{14}$, of the langasite-type structure from Pyrometamorphic rocks of the Hatrurim complex, Palestine," in *3rd European Mineralogical Conference EMC 2020*, p. 151, Book of Abstracts, Cracow, Poland, 2021.

[6] I. A. Andreev, "Single crystals of the Langasite family: an intriguing combination of properties promising for Acousto-electronics," *Technical Physics*, vol. 51, no. 6, pp. 758–764, 2006.

[7] I. S. Lyubutin, P. G. Naumov, B. V. Mill', K. V. Frolov, and E. I. Demikhov, "Structural and magnetic properties of the iron-containing Langasite family $A_3Mfe_3X_2O_{14}$ (A = Ba, SR; M = SB, Nb, TA; X = SI, GE) observed by Mössbauer spectroscopy," *Physical Review B*, vol. 84, p. 214425, 2011.

[8] I. S. Lyubutin, S. S. Starchikov, A. G. Gavriliuk, et al., "Magnetic phase separation and strong enhancement of the Neel temperature at high pressures in a new Multiferroic $Ba_3Tafe_3Si_2O_{14}$," *JETP Letters*, vol. 105, no. 1, pp. 26–33, 2017.

[9] M. M. Markina, B. V. Mill, G. Pristáš, et al., "$La_3Crge_3Be_2O_{14}$ and $Nd_3Crge_3Be_2O_{14}$: new magnetic compounds of the Langasite family," *Journal of Alloys and Compounds*, vol. 779, pp. 380–386, 2019.

[10] B. V. Mill and Yu. K. Pisarevsky, "Langasite-type materials: from discovery to present state," in *Proceedings of the 2000 IEEE/EIA International Frequency Control Symposium and Exhibition (Cat. No.00CH37052)*, pp. 133–144, Kansas City, MO, USA, 2000.

[11] S. S. Rathore, R. Nathawata, and S. Vitta, "A 'mixed' Dielectric response in Langasite $Ba_3Nbfe_3Si_2O_{14}$," *Physical Chemistry Chemical Physics*, vol. 23, pp. 554–562, 2021.

[12] A. A. Kaminskii, B. V. Mill, G. G. Khodzhabagyan, A. F. Konstantinova, A. I. Okorochkov, and I. M. Silvestrova, "Investigation of trigonal $(La_{1-x}Nd_x)_3Ga_5SiO_{14}$ crystals: I growth and optical properties," *Physica Status Solidi (A)*, vol. 80, no. 1, pp. 387–398, 1983. http://doi.wiley.com/10.1002/pssa.v80:1.

[13] I. S. Lyubutin, S. S. Starchikov, A. G. Gavriliuk, et al., "High pressure magnetic, structural, and electronic transitions in Multiferroic $Ba_3Nbfe_3Si_2O_{14}$," *Applied Physics Letters*, vol. 112, no. 24, 2018.

[14] B. H. T. Chai, A. N. P. Bustamante, and M. C. Chout, "A new class of ordered Langasite structure compounds," in *Proceedings of the 2000 IEEE/EIA International Frequency Control Symposium and Exhibition (Cat. No.00CH37052)*, pp. 163–168, Kansas City, MO, USA, 2000.

[15] K. Chen, C. Lin, S. Zhang, et al., "$A_3Te(Zn_2Ge)Ge_2O_{14}$ (A = SR, BA, and PB): new Langasite mid-infrared Nonlinear optical materials by rational chemical substitution, " *Chemistry of Materials*, vol. 33, no. 15, pp. 6012–6017, 2021.

[16] A. E. Lam, L. E. Groat, and T. S. Ercit, "The crystal structure of Dugganite, $Pb_3Zn_3Te_6+As_2O_{14}$," *The Canadian Mineralogist*, vol. 36, pp. 823–830, 1998.

[17] M. M. Markina, B. V. Mill, E. A. Zvereva, A. V. Ushakov, S. V. Streltsov, and A. N. Vasiliev, "Magnetic phase diagram and first-principles study of $Pb_3Teco_3V_2O_{14}$," *Physical Review B*, vol. 89, 2013.

[18] A. A. Kim, N. V. Zayakina, and V. F. Makhotko, "Kuksite, $PB_3Zn_3Teo_6(PO_4)_2$ and Cheremnykhite, $PB_3Zn_3Teo_6(VO_4)_2$ – new Tellurates from Kuranakh gold deposit (central Aldan, Southern Yakutia)," *Zapiski Vsesoyuznogo Mineralogicheskogo Obshchestva*, vol. 119, no. 5, pp. 50–57, n.d.

[19] S. A.Williams, "Khinite, Parakhinite, and Dugganite three new Tellurates from tombstone, Arizona," *American Mineralogist*, vol. 63, pp. 1016–10l9, 1978.

[20] S. J. Mills, U. Kolitsch, R. Miyawaki, L. A. Groat, and G. Poirier, "Joëlbruggerite, $PB_3Zn_3(Sb^{5+},Te^{6+})As_2O_{13}(OH,O)$, the SB^{5+} analog of Dugganite, from the black pine mine, Montana," *American Mineralogist*, vol. 94, no. 7, pp. 1012–1017, 2009.

[21] C. Ma, J. R. Beckett, E. L. H. Tissot, and G. R. Rossman, "New minerals in type A inclusions from Allende and clues to processes in the early solar system: Paqueite, $Ca_3TiSi_2(Al,TI,Si)3O_{14}$, and burnettite, $Cavalsio_6$," *Meteoritics & Planetary Science*, vol. 57, no. 6, pp. 1300–1324, 2022.

[22] E. Galuskin, I. O. Galuskina, V. Kamenetsky, et al., "First in situ terrestrial Osbornite (tin) in the Pyrometamorphic Hatrurim complex, Israel," *Lithosphere*, vol. 2022, no. 1, p. 8127747, 2022.

[23] E. V. Galuskin, J. Kusz, I. O. Galuskina, M. Książek, Ye. Vapnik, and G. Zieliński, "Discovery of terrestrial Andreyivanovite, FeCrP, and the effect of Cr and V substitution in Barringerite-Allabogdanite low-pressure transition," *American Mineralogist*, no. 2023, n.d.

[24] S. N. Britvin, M. N. Murashko, Ye. Vapnik, Yu. S. Polekhovsky, and S. V. Krivovichev, "Earth's Phosphides in Levant and insights into the source of Archean Prebiotic phosphorus," *Scientific Reports*, vol. 5, 2015.

[25] F. Hirsch, A. Burg, and Y. Avani, "Geological map of Israel 1:50 000 Arade sheet," *Geological Survey*, 2008.

[26] S. Gross, "The Mineralogy of the Hatrurim formation, Israel," *Bulletin of the Geological Survey of Israel*, vol. 70, pp. 1–80, 1977.

[27] A. Burg, Y. Kolodny, and V. Lyakhovsky, "Hatrurim-2000: the "mottled zone" Revisited, forty years later," *Israel Journal of Earth Sciences*, vol. 48, pp. 209–223, 1999.

[28] I. Novikov, Ye. Vapnik, and I. Safonova, "Mud volcano origin of the mottled zone, South Levant," *Geoscience Frontiers*, vol. 4, no. 5, pp. 597–619, 2013.

[29] C. Ma and A. N. Krot, "Hutcheonite, $Ca_3Ti_2(SiAl_2)O_{12}$, a new garnet mineral from the Allende meteorite: an alteration phase in a ca-al-rich inclusion," *American Mineralogist*, vol. 99, no. 4, pp. 667–670, 2014.

[30] A. P. Dudka and B. V. Mill', "X-ray diffraction study of a $Nd_3Ga_5SiO_{14}$ crystal at 295 and 90 K and the structural basis for Chirality," *Crystallography Reports*, vol. 59, no. 5, pp. 689–698, 2014.

[31] V. S. Gorelik, T. G. Golovina, and A. F. Konstantinova, "Raman scattering in Langasite-family crystals," *Crystallography Reports*, vol. 64, no. 2, pp. 287–291, 2019.

[32] C. M. Gray, D. A. Papanastassiou, and G. J. Wasserburg, "The identification of early condensates from the solar nebula," *Icarus*, vol. 20, no. 2, pp. 213–239, 1973.